ChemistryEurope
Excellence in Chemistry Research Worldwide

Research Article
doi.org/10.1002/ceur.202500337

www.journal.chemistry-europe.org

Hydrogen Bonding is Key Factor in Reversible NH_3 Uptake Causing Vapochromic and Magnetochemical Switching in Ni(II) Paddlewheel Complexes

Sebastian Rücker, Jörg A. Schachner, Sergey M. Borisov, Ferdinand Belaj, Silvia Carlotto,* Lidia Armelao, Antoine Dupé, and Nadia C. Mösch-Zanetti*

The bidendate ligands H**Pn^{Me}** (4-methyl-6-*tert*-butyl-3(2*H*)-thiopyridazine) and H**Pn^{tBu}** (4,6-di-*tert*-butyl-3(2*H*)-thiopyridazine) were coordinated to Ni(II) for the formation of paddlewheel (PW) complexes $[Ni_2(\mathbf{Pn^R})_4]$. Starting from $[NiCl_2(H\mathbf{Pn^{Me}})_4]$ (**1^{Me}**), the poorly soluble hexanuclear cluster $[Ni_6(\mathbf{Pn^{Me}})_{12}]$ (**2$^{Me'}$**) forms which is capable of binding NH_3 reversibly. The obtained monomeric PW complex $[Ni_2(\mathbf{Pn^{Me}})_4(NH_3)]$ (**3^{Me}**) shows vapochromism and magnetochemical switching. The third donor site in the pyridazine heterocycle **Pn^{Me}** is found to be a key factor for selective NH_3 uptake due to the ideal position of these additional nitrogen atoms in the second coordination sphere to form hydrogen bonds to NH_3. With excess NH_3 the PW core of **3^{Me}** collapses, and the octahedral bis–ammine complex $[Ni(\mathbf{Pn^{Me}})_2(NH_3)_2]$ (**4^{Me}**) is formed. Upon loss of NH_3, **3^{Me}** is reformed. All three compounds **2$^{Me'}$**, **3^{Me}** and **4^{Me}** have a very different color in solution or suspension, which allows for basic sensing properties. Quantum mechanical calculations on complexes clarify the preference for the N site over sulfur in coordinating small molecules. The influence of hydrogen bonding on this preference is quantitatively emphasized, providing confirmation of the high selectivity of these systems for NH_3. In contrast to H**Pn^{Me}**, with the bulkier ligand H**Pn^{tBu}**, two H**Pn^{tBu}** molecules coordinate to $NiCl_2$, giving the tetrahedral complex $[NiCl_2(H\mathbf{Pn^{tBu}})_2]$ (**5^{tBu}**) while a PW complex was not observed.

1. Introduction

A paddlewheel (PW) complex of the general formula $[M_2(XY)_4]$ (XY = bidentate, bridging ligand) consists of two metal centers that are coordinated by four bidentate ligands which are bridging the two metals.[1–8] Compared with other metals, relatively few group 10 PWs have been published and structurally characterized (Pt ≈ 100; Pd, Ni < 20 each). For Ni_2-based PW complexes, both symmetrically bridged by *O, O*-,[9] *S, S*-[10–14] or *N, N*-[15–20] type ligands, as well as asymmetrically bridged by *S, O*-,[21,22] *N, O*-[23] or *S, N*-[24,25] ligands have been reported. PW complexes of Ni, Pd, or Pt can display interesting magnetic properties. Based on the arising square-planar ligand field and the d^8 electronic configuration in the predominant M(II) oxidation state, metal–metal bonds should be absent in the respective PW complexes.[17,19,26] This bonding situation has been confirmed for all Pd(II) and Pt(II) PW complexes. For Ni_2-PWs, the coordination of an additional axial ligand at one or both Ni centers is often observed, resulting in a change of ligand field to square-pyramidal, which causes a switch of the magnetic state.[15–18,24,25]

Complexes for which both a diamagnetic state (with spin quantum number S = 0) and a paramagnetic state (e.g. S = 1) can be realized by reversible coordination of a ligand L are referred to as spin crossover (SCO) metal complexes.[27,28] The effect of magnetic bistability was mostly found in solid-state materials and/or at very low temperatures.[29,30] Over the last years though, more examples of discrete complexes that show SCO properties in solution at room temperature have been disclosed.[27,28,30–34] The magnetic crossover also influences other physical properties of the complexes. Often, the color of the complex changes upon de-/coordination of the L ligand, resulting in an effect termed vapochromism.[34–37]

S,N-Bridged Ni_2-PWs have been reported either with[24] or without[25,38,39] axially bound ligand. The first example where both

S. Rücker, J. A. Schachner, F. Belaj, A. Dupé, N. C. Mösch-Zanetti
Institute of Chemistry
University of Graz
Schubertstrasse 1, 8010 Graz, Austria
E-mail: nadia.moesch@uni-graz.at

S. M. Borisov
Institute of Analytical Chemistry and Food Chemistry
Graz Institute of Technology
Streymayrgasse 9, 8010 Graz, Austria

S. Carlotto, L. Armelao
Department of Chemical Sciences, University of Padova
via F. Marzolo 1, 35131 Padova, Italy
E-mail: silvia.carlotto@unipd.it

S. Carlotto
Institute of Condensed Matter Chemistry and Energy Technologies (ICMATE)-CNR
c/o, via F. Marzolo 1, 35131 Padova, Italy

L. Armelao
Department of Chemical Sciences and Materials Technologies (DSCTM)-CNR
Piazzale A. Moro 7, 00185 Roma, Italy

Supporting information for this article is available on the WWW under https://doi.org/10.1002/ceur.202500337

Research Article
doi.org/10.1002/ceur.202500337

situations were obtained in the same PW core was reported by our group in 2021.[40] By reacting the *S,N*-bidentate ligand 6-*tert*-butyl-pyridazine-3-thione (H**Pn^{H}**) (**Scheme 1**)[41–46] with $NiCl_2$, the diamagnetic PW complex $[Ni_2(\mathbf{Pn^H})_4]$ (**2^{H}**) was obtained.[40] We found remarkable coordination properties towards NH_3, yielding the PW complex $[Ni_2(\mathbf{Pn^H})_4(NH_3)]$ (**3^{H}**). The latter is the first example of an ammonia coordinated nickel paddlewheel. Furthermore, it is paramagnetic after NH_3 coordination ($S = 1$) and its formation is accompanied by a significant color change rendering **2^{H}** the first Ni_2-PW complex to show both vapochromism and spin crossover (magnetic bistability). De-coordination of NH_3 is triggered by vacuum, which reverts $[Ni_2(\mathbf{Pn^H})_4(NH_3)]$ to $[Ni_2(\mathbf{Pn^H})_4]$ under retention of the PW core. The analogous reactivity was also found in fabricated thin, gas-permeable polyurethane films (Hydromed D4), with the encapsulated PW complex which retained its NH_3-sensing capability.[40] The uptake (dipping in an NH_3 solution) and release (rinsing with H_2O) of NH_3 proved to be fully reversible over several cycles, demonstrating basic sensing properties.[47] However, based on the state-of-the-art sensing requirements,[47] our molecular paddlewheel complex does not fulfill these criteria. For example, the difference in wavelengths between the ammonia coordinated and the parent Ni_2-PW should be larger and the sensitivity higher. We were therefore interested in further investigating the coordination chemistry of 4-Me and 4-*t*Bu substituted pyridazine-3-thione ligands H**Pn^{Me}**[48] and H**Pn^{tBu}** toward nickel(II). Here, we present a combined synthetic and theoretical study of the propensity for PW formation in the series of the H**Pn^{R}** ligands (R = H, Me, *t*Bu) with nickel(II) and small molecule coordination (ammonia and water) at both nickel sites by focusing the attention on their vapochromism and spin crossover properties.

2. Results and Discussion

2.1. Formation of Paddlewheel Complexes using HPn^{Me}

In analogy to H**Pn^{H}**, upon reaction of 4 equiv of H**Pn^{Me}** with $NiCl_2 \cdot 6H_2O$ in EtOH, the octahedral complex $[NiCl_2(\mathbf{HPn^{Me}})_4]$ (**1^{Me}**) is obtained (**Scheme 2**). The chlorido ligands occupy the apical positions while the four pyridazine-thione ligands are coordinated in a monodentate fashion in the equatorial plane via their sulfur atom. All four H**Pn^{Me}** ligands remain protonated, with the N-H protons forming hydrogen bonds to the chlorido ligands.

Complex **1^{Me}** can be isolated in 84% yield by simple removal of EtOH and washing of the crude product with pentane. Its octahedral structure was confirmed by single crystal X-ray diffraction analysis.[49] A molecular view and crystallographic data can be found in the Supporting Information (Figure S9, Table S1,S4, and S5, Supporting Information). The expected paramagnetism of **1^{Me}** was observed both by magnetic susceptibility measurements using a Gouy balance ($\chi_M = 5.45 \times 10^{-8}$ m^3 mol^{-1}; $\mu_{eff} = 3.17$ (2.32 unpaired e$^-$) and by ^{1}H NMR spectroscopy which only showed broadened and shifted peaks suggesting the presence of a high spin Ni(II) center (Figure S1, Supporting Information). When a second equiv of $NiCl_2 \cdot 6H_2O$ and 4 equiv of NaH were added to **1^{Me}** in MeOH, after heating, a brownish precipitate of **2$^{Me'}$** formed (Scheme 2). Compound **2$^{Me'}$** is poorly soluble in all common organic solvents, which hindered meaningful characterization in solution. Nevertheless, by slow evaporation from a saturated $CHCl_3$ solution, single crystals were obtained allowing X-ray diffraction analysis.[49] Surprisingly, instead of the expected PW structure $[[Ni_2(\mathbf{Pn^{Me}})_4]$ (**2^{Me}**), a trimeric structural isomer was obtained, namely a hexanuclear, cyclic,

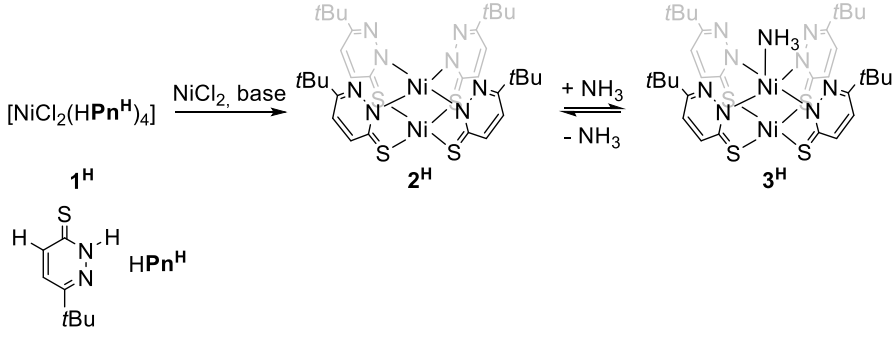

Scheme 1. Reversible ammonia coordination in $[Ni_2(\mathbf{Pn^H})_4]$ (**2^{H}**).[40]

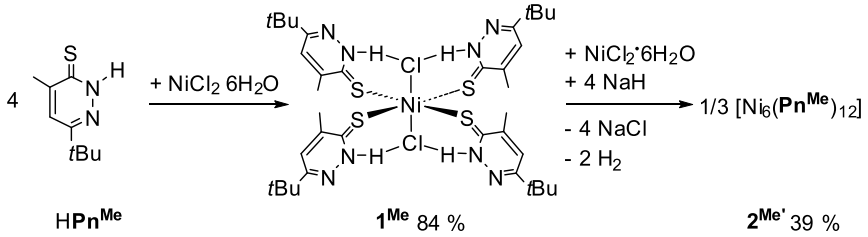

Scheme 2. Synthesis of $[NiCl_2(\mathbf{HPn^{Me}})_4]$ (**1^{Me}**) and hexanuclear $[Ni_6(\mathbf{Pn^{Me}})_{12}]$ (**2$^{Me'}$**).

Research Article
doi.org/10.1002/ceur.202500337

torus-shaped structure of the formula $[Ni_6(\mathbf{Pn^{Me}})_{12}]$ ($\mathbf{2^{Me'}}$) (**Figure 1**, S10,S11, Supporting Information).

The octahedral coordination of each of the six Ni atoms causes $\mathbf{2^{Me'}}$ to be paramagnetic. The number of unpaired electrons was determined to be approximately 6 by magnetic susceptibility measurements, lower than the theoretically possible number of 12 if all six Ni atoms were magnetically isolated. This seemingly contradicting result could be caused by an inhomogeneity of the sample, varying amounts of embedded solvent molecules in the crystalline samples as well as antiferromagnetic coupling, as observed in other PW and polynuclear Ni complexes.[9,50–53] The synthesis of $\mathbf{2^{Me'}}$ can also be accomplished without the isolation of $\mathbf{1^{Me}}$ when the base NaH is added directly to the respective amounts of $\mathbf{HPn^{Me}}$ and $NiCl_2 \cdot 6H_2O$. Although the choice of MeOH as reaction solvent seems counterintuitive here, it consistently gave the best results and highest yields of $\mathbf{2^{Me'}}$. The formation of other, differently sized cyclic or acyclic oligomers cannot be excluded. The very low solubility in various organic solvents of $\mathbf{2^{Me'}}$ hampers its detailed study but supports the formation of the Ni_6 oligomer as the PW complex $[Ni_2(\mathbf{Pn^{Me}})_4]$ is expected to be more soluble. This is in stark contrast to ligand $\mathbf{Pn^H}$, where predominantly the PW $[Ni_2(\mathbf{Pn^H})_4]$ ($\mathbf{2^H}$) is formed.

Even though the ligand $\mathbf{HPn^{Me}}$ did not allow for the isolation of a monomeric PW complex of type $[Ni_2(\mathbf{Pn^{Me}})_4]$, we were delighted to observe a significant color change upon exposure of solid $\mathbf{2^{Me'}}$ to NH_3. If gaseous NH_3 is bubbled through a suspension of poorly soluble $\mathbf{2^{Me'}}$, in $CHCl_3$ or CH_2Cl_2, a gradual color change from brownish to red was observed upon dissolution of the solids giving a bright red solution (**Scheme 3**). Evaporation of the solvents gave the analytically pure PW

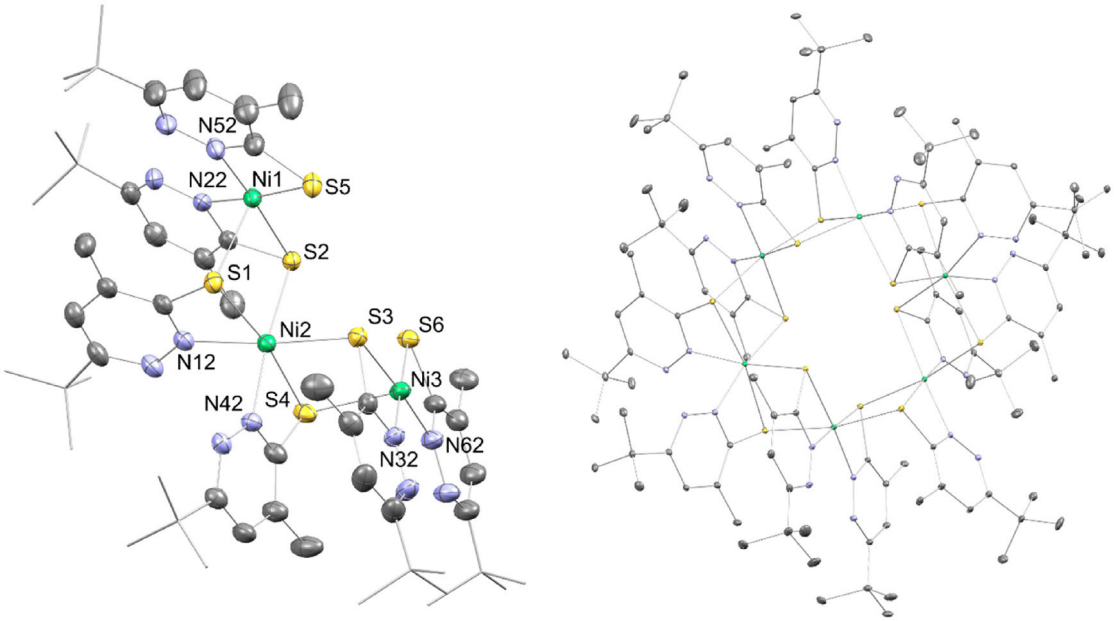

Figure 1. Right: molecular view of the asymmetric unit of the complex $[Ni_6(\mathbf{Pn^{Me}})_{12}]$ ($\mathbf{2^{Me'}}$). The probability ellipsoids are drawn at the 50% probability level. The H atoms and solvent molecules were omitted for clarity. *tert*-Butyl groups of the ligands are drawn as wireframe for clarity. Left: Molecular view of the hexameric metal complex $[Ni_6(\mathbf{Pn^{Me}})_{12}]$ ($\mathbf{2^{Me'}}$). The atoms are drawn with arbitrary radii, the H atoms were omitted for clarity.

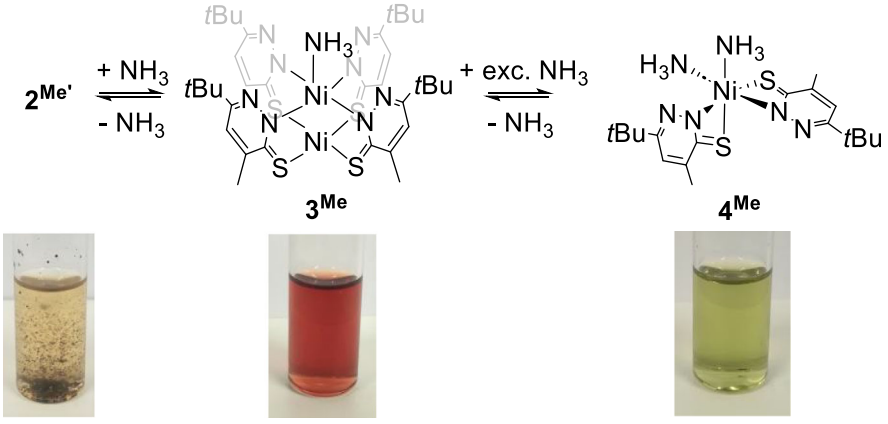

Scheme 3. Reversible color changes upon exposure of $\mathbf{2^{Me'}}$ to NH_3 (in CH_2Cl_2).

Research Article
doi.org/10.1002/ceur.202500337

$[Ni_2(\mathbf{Pn^{Me}})_4(NH_3)]$ ($\mathbf{3^{Me}}$) with a coordinated ammonia molecule. Formation of $\mathbf{3^{Me}}$ is also observed if a slight excess of aqueous ammonia is added to the suspension of $\mathbf{2^{Me'}}$. Single crystals were obtained from a saturated $CHCl_3$ solution allowing for X-ray diffraction analysis which confirms the formation of the paddlewheel, with the ammonia molecule forming at least two short H-bonds with two available nitrogen atoms of the $\mathbf{Pn^{Me}}$ ligands (**Figure 2** and S12, Supporting Information).[49]

For quantification, NH_3 gas was added stepwise by syringe to a stirred suspension of 20 mg of $\mathbf{2^{Me'}}$ in 6 mL CH_2Cl_2. Starting with 0.2 equiv. up to 3 equiv. of NH_3 gas (with respect to the paddlewheel or 0.6 equiv. with respect to the hexamer) were added to the solution, and the reaction was monitored using UV-Vis spectroscopy. Spectra were recorded after 5 and 10 min of addition. A band at 529 nm corresponding to $\mathbf{3^{Me}}$ appears with the addition of the first 0.2 equiv. of NH_3 and gradually increases until 3 equiv. of NH_3 were added and all hexamer $\mathbf{2^{Me'}}$ was dissolved (Figure S6, Supporting Information). The absorption correlates linearly until one equiv. of ammonia per paddlewheel (0.5 equiv. per Ni) was added (Figure S7, Supporting Information). This demonstrates the high sensitivity of the hexamer toward ammonia as a substoichiometric addition of NH_3 gas leads to $\mathbf{3^{Me}}$ and a threefold excess is enough for complete conversion. The expected paramagnetism based on the solid-state structure of $\mathbf{3^{Me}}$ was confirmed by ^{1}H NMR spectroscopy as well as magnetic susceptibility measurements (Figure S2, Supporting Information).

Interestingly, when a large excess of ammonia was added to a suspension of $\mathbf{2^{Me'}}$ or a solution of $\mathbf{3^{Me}}$ in dichloromethane, a color change to yellow-green (Scheme 3) occurred. Using aqueous ammonia, we found that at least 100 equiv. are required while with 50 equiv. no color change was observed. The novel green species was identified as the bis–ammine complex $[Ni(\mathbf{Pn^{Me}})_2(NH_3)_2]$ ($\mathbf{4^{Me}}$) (Scheme 3). Its isolation proved to be challenging as $\mathbf{4^{Me}}$ is very sensitive to loss of NH_3, both in solution and solid state, upon which it cleanly reverts to $\mathbf{3^{Me}}$. For example, under a vacuum of 10^{-2} mbar at 25 °C, $\mathbf{4^{Me}}$ reacts to $\mathbf{3^{Me}}$ within an hour.

Hence, the bis–ammine complex $\mathbf{4^{Me}}$ was best isolated in substance by carefully dry-blowing a saturated CH_2Cl_2 solution with a stream of gaseous NH_3. A green solution of $\mathbf{4^{Me}}$ in CH_2Cl_2 ($\approx$10 mg ml^{-1}) reverts to a red solution of $\mathbf{3^{Me}}$ within 20 min (Scheme 3). Solid samples of $\mathbf{4^{Me}}$ can only be stored for prolonged times under an NH_3 atmosphere. Suitable single crystals for X-ray diffraction analysis were obtained by slow evaporation of a green solution of $\mathbf{4^{Me}}$ in CH_2Cl_2 which was layered with a conc. aqueous solution of NH_3. Before mounting them on the diffractometer, the crystals must be kept under a layer of conc. aqueous NH_3. The solid-state analysis of $\mathbf{4^{Me}}$ confirmed the octahedral surrounding of the Ni(II) center with two NH_3 ligands being *cis* to each other (Figure S13, Supporting Information).

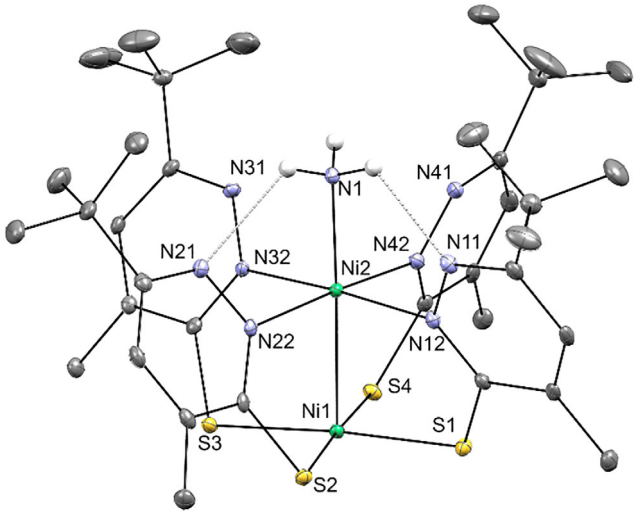

Figure 2. Molecular view of $[Ni_2(\mathbf{Pn^{Me}})_4(NH_3)]$ ($\mathbf{3^{Me}}$). The probability ellipsoids are drawn at the 30% probability level. Only one position for the disordered H atoms of the ammine ligand is shown, the other H atoms were omitted for clarity.

2.2. Formation of Nickel Complexes Using $\mathbf{HPn^{tBu}}$

The coordination chemistry of ligand $\mathbf{HPn^{tBu}}$ differs significantly from that of $\mathbf{HPn^{H}}$ and $\mathbf{HPn^{Me}}$. The reaction of 4 equiv of $\mathbf{HPn^{tBu}}$ with $NiCl_2 \cdot 6H_2O$ led to $[NiCl_2(\mathbf{HPn^{tBu}})_2]$ ($\mathbf{5^{tBu}}$) together with two equiv of unreacted $\mathbf{HPn^{tBu}}$, regardless of the applied reaction conditions (**Scheme 4**). By applying the correct stoichiometry of $Ni{:}\mathbf{HPn^{tBu}} = 1{:}2$, complex $\mathbf{5^{tBu}}$ could be isolated in 89% yield as a brown-green solid. Single crystal X-ray diffraction analysis revealed a tetrahedral coordination geometry around the Ni(II) center, with two sulfur and two chloride atoms coordinated to Ni.[49] The NH moieties are involved in hydrogen bonds to the chloride ligands (Figure S14, Supporting Information).

The tetrahedral coordination of a Ni(II) center is a rather rarely observed geometry.[54–58] The steric bulk imposed by the second *t*Bu group in $\mathbf{HPn^{tBu}}$ most likely does not allow for the coordination of four ligands to the Ni center as observed with $\mathbf{HPn^{Me}}$. When two equiv of NaH are added to $\mathbf{5^{tBu}}$ deprotonation of the $\mathbf{HPn^{tBu}}$ ligands occurs, resulting in bidentate coordination of $\mathbf{Pn^{tBu}}$ forming $[Ni(\mathbf{Pn^{tBu}})_2]$ ($\mathbf{6^{tBu}}$). After work-up as described in the supporting information, the latter was isolated in 71% yields as a green solid. Complex $\mathbf{6^{tBu}}$ is quite soluble in chlorinated solvents and toluene leading to deep yellow-green solutions. Single crystals analyzed by X-ray diffraction revealed a square planar coordination around the Ni(II) center, with the two $\mathbf{Pn^{tBu}}$ moieties in a *trans* arrangement (Figure S15, Supporting Information).[49] In accordance with this solid-state structure, complex $\mathbf{6^{tBu}}$ was found to be diamagnetic. Finally, $\mathbf{6^{tBu}}$ did not react with NH_3 consistent with no observable color change. The analytical data collected together with the lack of vapochromic behavior toward NH_3 led us to conclude that ligand $\mathbf{HPn^{tBu}}$ does not allow for the formation of PW complexes.

2.3. Theoretical Studies on Binding Properties, Spin Crossover, and Reactivity

To rationalize the different behavior of the paddlewheel complexes in the absence and presence of small molecules in the series of the $\mathbf{HPn^{R}}$ ligands (R = H, Me, *t*Bu) with nickel(II),

Research Article
doi.org/10.1002/ceur.202500337

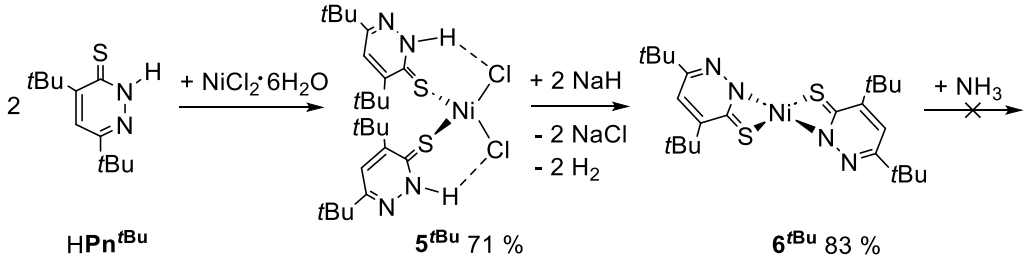

Scheme 4. Synthesis of mononuclear complexes $[NiCl_2(HPn^{tBu})_2]$ (5^{tBu}) and $[Ni(Pn^{tBu})_2]$ (6^{tBu}).

theoretical investigations by using quantum mechanical calculations were performed with the Pn^H system, especially to compare our previously published $[Ni_2(Pn^H)_4]$ (2^H) and $[Ni_2(Pn^H)_4(NH_3)]$ (3^H)[40] with $2^{Me'}$ and 3^{Me} (Scheme 3). All calculations are performed by using the B3LYP functional with the inclusion of dispersion correction (see Supporting Information). First, the selectivity of the coordination of NH_3 for two possible nickel sites (at the N side or the S side) was studied. Indeed, despite the presence of two Ni atoms in the PW complexes, the NH_3 coordination is only observed on the side where the nickel is coordinated by four nitrogen atoms of the Pn^H ligands (Ni-4N). Moreover, the magnetic property was investigated. The nickel(II) ion can have a high spin (HS) (with two unpaired electrons) and a low spin (LS) state (without unpaired electrons). The spin crossover due to the coordination of NH_3 is experimentally observed for 2^H and $2^{Me'}$, forming the HS state in both cases upon coordination. For the former, SQUID magnetic measurements have shown that only the Ni atom, where the coordination of NH_3 takes place, is involved.[40] In the absence of NH_3, no spin state changes are observed.

To explain the selectivity and the spin crossover properties, the binding energies for both Ni sites as well as both spin states are calculated by comparing the energy differences between the energy of the paddlewheel complex with coordinated NH_3 (3^H) and the sum of the energies of the precursor complex (2^H) and an isolated NH_3 molecule. The binding energies of the NH_3 for HS states at the 4N- and 4S-sides are −18.75 and −14.85 kcal mol^{-1}, respectively (**Table 1**). Adding the NH_3 molecule at the 4S-side is thus energetically less favored by 3.9 kcal mol^{-1}, justifying the experimental evidence. However, similar calculations considering LS states reveal a preference for the 4S-side by 5.37 kcal mol^{-1} (Table 1). In agreement with experimental data, calculations show that adding NH_3 at the more stable 4N-side to give 3^H or 3^{Me} causes the Ni(II) spin crossover from the LS to the HS state. In both compounds, the HS state is significantly more stable than the LS one of −18.42 kcal mol^{-1} for 3^H and −17.14 kcal mol^{-1} for 3^{Me} (Table 1). Optimized geometries for NH_3 coordination at the 4N-side for LS and HS states for H and Me substitutes are reported in Figures S17 and S18, Supporting Information. Analogous calculations were performed with NH_3 binding on the 4S-side: the HS state is more stable than the LS state for 3^H (−9.16 kcal mol^{-1}), however HS and LS states for 3^{Me} are almost identically stable.

Energy decomposition analysis with the combination of natural orbitals for chemical valence (EDA-NOCV, see computational details in SI) analysis on the interaction between the fragment ammonia and the paddlewheel (in 3^H/3^{Me}) has been performed, including comparison of HS and LS state configurations. EDA-NOCV offers valuable insight into the relative contributions of electrostatic and orbital interactions, as well as the role of hydrogen bonding in modulating ligand binding across spin states. The analysis reveals a marked spin-state dependence in the bonding interaction, in agreement with experimental data. NH_3 binds preferentially and more strongly in the HS state due to stronger orbital and electrostatic interactions, despite higher steric repulsion (Table S13, Supporting Information). The LS state does not support favorable NH_3 coordination. Similar results are obtained for 3^{Me} A more detailed description of the weight of each term composing the interaction energy is reported in the SI. However, this method is not suitable to explain the experimentally observed preference for coordination at the 4N over the 4S site and to fully quantify the role of the H–bond interaction.

Table 1. NH_3 or H_2O binding energies (in kcal/mol) in $[Ni_2(Pn^H)_4(L)]$ (L = NH_3 (3^H) or H_2O) and $[Ni_2(Pn^{Me})_4(L)]$ (L = NH_3 (3^{Me}) or H_2O) at the 4N- and 4S-side for both the diamagnetic (LS) and paramagnetic (HS) spin state. Δ_{spin} refers to the energy differences of the two spin states and Δ_{site} to those of the coordination site.

L	Coordination site	$[Ni_2(Pn^H)_4(L)]$			$[Ni_2(Pn^{Me})_4(L)]$		
		LS	HS	Δ_{spin}	LS	HS	Δ_{spin}
NH_3	4N-side	−0.32	−18.75	−18.42	1.00	−18.14	−17.14
	4S-side	−5.69	−14.85	−9.16	−5.28	−5.30	−0.02
	Δ_{site}	5.37	−3.90	–	4.28	−12.84	–
H_2O	4N-side	−11.76	−13.84	−2.08	−12.09	−13.25	−1.16
	4S-side	−5.07	−5.10	−0.03	−5.28	−5.30	−0.02
	Δ_{site}	−6.69	−8.74	–	−6.81	−7.95	–

Research Article
doi.org/10.1002/ceur.202500337

Energy decomposition analysis with the combination of natural orbitals for chemical valence (EDA-NOCV, see computational details in SI) was employed to dissect the interaction between NH_3 and the dinuclear fragments $[Ni_2(\mathbf{Pn^{Me}})_4]$ and $[Ni_2(\mathbf{Pn^{Me}})_4]$ (see Table S13, Supporting Information). The results underscore the interplay of spin state and ligand substitution in governing the magnitude and nature of the NH_3 interaction. Across both complexes, NH_3 coordination leads to stabilization, with interaction energies substantially stronger in the HS state (≈–41 to –42 kcal mol^{-1}) than in the LS state (≈–8 to –9 kcal mol^{-1}). This difference arises from more effective $\sigma(NH_3 \rightarrow Ni)$ donation in the HS configuration, where partially filled d-orbitals provide accessible acceptor states. In contrast, in the LS state orbital interactions collapse (fivefold weaker), leaving binding dominated by residual electrostatics. Pauli repulsion represents the principal destabilizing component, with higher values in the HS state (≈110 kcal mol^{-1}) reflecting enhanced electron–electron repulsion from unpaired d-electrons, while substantially lower values in LS (≈45 kcal mol^{-1}) mirror reduced overlap. Substituent effects are modest but systematic: The methyl substituent enhances both electrostatic stabilization (HS: –83.2 → –84.0 kcal mol^{-1}; LS: –31.2 → –32.4 kcal mol^{-1}) and orbital interactions (HS: –58.0 → –59.3 kcal mol^{-1}; LS: –11.9 → –12.9 kcal mol^{-1}). This reflects the electron-donating character of the Me group, which increases polarization of the Ni_2 fragment, promotes σ donation from NH_3, and subtly strengthens the overall coordination. Dispersion remains essentially invariant (≈–9 to –10 kcal mol^{-1}), consistent with its origin in the aromatic framework. In terms of hydrogen bonding, the EDA indicates that contributions emerge primarily through the electrostatic and orbital components. The stronger electrostatics in $[Ni_2(\mathbf{Pn^{Me}})_4(NH_3)]$ suggest that the methyl substituent indirectly reinforces H-bonds by increasing electron density on the pyridazine nitrogen atoms (confirmed by Mulliken charge analysis, Figure S16, Supporting Information), thereby strengthening N–H···N interactions. Orbital contributions, associated with polarization and charge delocalization within the H-bonding network, are also slightly enhanced in the methyl substituted system. Spin state exerts a dominant effect: In the HS state, robust electrostatic and orbital terms support significant H-bond stabilization, whereas in the LS state, both contributions collapse, consistent with the reduced donor–acceptor flexibility of the low-spin configuration. In summary, EDA reveals a clear hierarchy of effects: (i) Spin state dictates the overall magnitude of NH_3 interaction, with HS strongly favored; (ii) ligand substitution fine-tunes the electrostatic and orbital components, with methyl groups modestly but systematically enhancing interaction; and (iii) hydrogen bonding emerges as a cooperative stabilizing factor, primarily electrostatic in nature but reinforced by polarization effects in the Me–substituted complex. Together, these findings rationalize the experimentally observed stronger NH_3 coordination in $[Ni_2(\mathbf{Pn^{Me}})_4(NH_3)]$ relative to $[Ni_2(\mathbf{Pn^{H}})_4(NH_3)]$, while underscoring the dual control of spin state and ligand electronics on metal–ligand binding.

The experimental selectivity can be further investigated by quantifying the electrophilicity of the two Ni atoms in $\mathbf{2^H}$. The electrophilic condensed Fukui function or simply condensed Fukui function f_k^+[59] (see computational details) reflects the reactivity of a site: the higher the function, the higher the capability to accept electrons. It serves as the fundamental density-based reactivity indicator for the location where the molecule is most susceptible to nucleophilic attack. In our case, the more electrophilic Ni atom should be the preferred coordination site for NH_3. Unexpectedly, the calculated f_k^+ for Ni at the 4S-side in $\mathbf{2^H}$ is significantly higher (0.007) than for the Ni at the 4N-side (0.002). Thus, the 4S-side should be the preferred coordination site based only on the Ni electrophilicity. In the literature, coordination compounds with a NiS_4N cores are indeed known.[60] This result contrasts with experimental findings suggesting additional influences. As coordination of NH_3 in $\mathbf{3^H}$ and $\mathbf{3^{Me}}$ involves the formation of two short NH···N hydrogen bonds and one longer one (Figures S17 and S18, Supporting Information), we hypothesized that such H-bonds are the main factor for the selectivity and stability of the complexes. In these PW, H-bonds are possible at the Ni 4N-side, while this is impossible at the 4S-side. A model system in which the original structural arrangement on $\mathbf{2^H}$ is maintained but the pyridazines are replaced by pyridines ($\mathbf{2^{Py}}$, Figure S19, Supporting Information) was used to verify this hypothesis. In such a paddlewheel, no additional N atoms in the ligands are available for H-bond formation to coordinate NH_3 at the 4N-side. For this model and in agreement with the calculated condensed Fukui function f_k^+, the addition of NH_3 at the Ni 4S-side in $\mathbf{2^{Py}}$ is slightly more stable than the Ni 4N-side by 0.5 kcal mol^{-1} (**Table 2**). This result supports our hypothesis and confirms the crucial role of the H-bond in stabilizing the Ni 4N- over the 4S-side. Interestingly, if NH_3 cannot form H-bonds, as in $\mathbf{2^{Py}}$, there is indeed no preferred binding site. Furthermore, a comparison of the NH_3 binding energies of $[\mathbf{2^{Py}}(NH_3)]$ ($\mathbf{3^{Py}}$) to those of $\mathbf{3^H}$ provides an estimation of the share of the H–bond interaction of the total bonding energy. Results show that the binding energy only due to the NH_3-Ni interaction in $\mathbf{3^{Py}}$ is lower than the one in $\mathbf{3^H}$ (−8.27 kcal mol^{-1} at the 4N-side and −3.90 kcal mol^{-1} at the 4S-side; Table 2). Since binding NH_3 at the Ni 4N-side in $\mathbf{3^H}$ involves three H-bonds, the resulting energy per H-bond is 2.76 kcal mol^{-1} (8.27/3). This value is in perfect agreement with the literature where in the NH_3-NH_3 dimer the H-bond is calculated around 2.5 kcal mol^{-1} with a MP2/6–31++G(d, p) level of theory.[61]

The reactivities of $\mathbf{2^H}$ and $\mathbf{2^{Me'}}$, respectively, toward the addition of NH_3 are very similar, while a striking difference is observed when $\mathbf{3^H}$ and $\mathbf{3^{Me}}$, respectively, react with excess NH_3 leading only for the latter to the bis–ammine complex $[Ni(\mathbf{Pn^{Me}})_2(NH_3)_2]$ ($\mathbf{4^{Me}}$). Calculations on both complexes, $\mathbf{4^{Me}}$ and the not experimentally observed $\mathbf{4^H}$, show the HS to be more stable than the LS states

Table 2. Binding energies (in kcal/mol) for NH_3 in $[Ni_2(\mathbf{Pn^H})_4(NH_3)]$ and $[Ni_2(\mathbf{Pn^{Py}})_4(NH_3)]$ together with the difference between the values for HS configuration.

Coordination site	$[Ni_2(\mathbf{Pn^H})_4(NH_3)]$	$[Ni_2(\mathbf{Pn^{Py}})_4(NH_3)]$	Difference
4N-side	−18.75	−10.48	−8.27
4S-side	−14.85	−10.95	−3.90

Research Article
doi.org/10.1002/ceur.202500337

(10.60 kcal mol^{-1} for $\mathbf{4^H}$ and 15.94 kcal mol^{-1} for $\mathbf{4^{Me}}$). A reason for the different reactivity can be obtained by comparing the stability energies of $\mathbf{4^H}$ or $\mathbf{4^{Me}}$ to those of $\mathbf{3^H}$ or $\mathbf{3^{Me}}$ and one molecule of NH_3. The comparison reveals $\mathbf{4^{Me}}$ to be more stable than $\mathbf{3^{Me}}$ by over 3 kcal mol^{-1} explaining its formation. In contrast, such a stability increase cannot be found with $\mathbf{4^H}$ explaining why it is not formed.

2.4. Studies on the Vapochromic Behavior: Experiment and Theory

As mentioned above, hexanuclear complex $\mathbf{2^{Me'}}$ reacts with gaseous NH_3 when suspended in CH_2Cl_2 or $CHCl_3$ under the formation of the PW complex $\mathbf{3^{Me}}$. The conversion to $\mathbf{3^{Me}}$ occurs also upon exposing the finely dispersed solid of $\mathbf{2^{Me'}}$, to gaseous NH_3, apparent by a color change to bright red after several minutes. The ^{1}H NMR spectrum of the latter in $CDCl_3$ is identical to that of isolated $\mathbf{3^{Me}}$, supporting reactivity in the solid state. Ammonia coordination was found to be reversible: If a red $CHCl_3$ solution of $\mathbf{3^{Me}}$ was left standing for over 16 h, a gradual de-coloration and precipitation of the brown solid of $\mathbf{2^{Me'}}$ was observed. In contrast, in the solid state at ambient pressure and room temperature, $\mathbf{3^{Me}}$ retains its characteristic red color for several months. Only upon applying vacuum (10^{-2} mbar) and temperature (100 °C), the solid material of $\mathbf{3^{Me}}$ changed color to brownish within 3 h, finally giving $\mathbf{2^{Me'}}$. The analogous reaction $[Ni_2(\mathbf{Pn^H})_4(NH_3)]$ ($\mathbf{3^H}$) was found to be faster, as thermal treatment at 110 °C for 1 h led to full conversion to $\mathbf{2^H}$.[38] Interestingly, NH_3 coordination/decoordination experiments, repeated multiple times, show full reversibility, without apparent decomposition of the respective complexes.

The calculated binding energies for NH_3 at $\mathbf{3^H}$ and $\mathbf{3^{Me}}$ reveal the latter to be slightly more stable (0.6 kcal mol^{-1}, Table 1), in contrast to experimental findings. However, it is well established that the energy accuracy of DFT is limited to approximately 2 kcal mol^{-1},[62] so this difference is not significant. The Ni-(NH_3) bond lengths are also similar between the two complexes (Table S14, Supporting Information). Thus, to better quantify the strength of the N–Ni bond in NH_3-Ni complexes and to better highlight the effect of ligand substitution on NH_3 coordination, the Mayer bond order (MBO)[63] values were calculated for the Ni-(NH_3) bond. A larger MBO is found for $\mathbf{3^{Me}}$ (0.5447) versus $\mathbf{3^H}$ (0.5340). These values clearly indicate, in agreement with experimental observations, that NH_3 coordination is strengthened upon substituting $\mathbf{Pn^H}$ by $\mathbf{Pn^{Me}}$ (Table S14, Supporting Information). This trend can be rationalized by examining the electronic structure, particularly the Mulliken charge distribution. As illustrated in Figure S16, Supporting Information, the $\mathbf{Pn^{Me}}$ ligand, although not directly engaged in hydrogen bonding, increases the negative charge on the nitrogen atoms involved in H-bonds (from –0.163e in $\mathbf{Pn^H}$ to –0.176e in $\mathbf{Pn^{Me}}$). Moreover, variations in the charge density on the nitrogen atoms directly coordinated to Ni significantly affect the overall stability of the complex. Taken together, these results demonstrate that ligand substitution subtly but decisively modulates both the hydrogen-bonding network and the metal–ligand interactions, thereby providing a consistent rationale for the experimentally observed differences in NH_3 coordination strength.

The conversion of yellow-green $\mathbf{4^{Me}}$ ($\lambda_{max}(CH_2Cl_2) = 582$ nm) to $\mathbf{3^{Me}}$ ($\lambda_{max}(CH_2Cl_2) = 529$ nm) could be followed by UV-Vis spectroscopy and occurred within 30 min (Figure S8, Supporting Information). The different molecular stoichiometry of $[Ni(\mathbf{Pn^{Me}})_2(NH_3)_2]$ ($\mathbf{4^{Me}}$) and $[Ni_2(\mathbf{Pn^{Me}})_4(NH_3)]$ ($\mathbf{3^{Me}}$) explains the absence of an isosbestic point for this conversion. An intermediate such as $[Ni(\mathbf{Pn^{Me}})_2(NH_3)]$ was not observed. The formation of a monomeric species similar to $\mathbf{4^{Me}}$ but with only one or no coordinated ammonia from $\mathbf{3^{Me}}$ is found to be unfavored from a computational point of view of over 30 kcal/mol calculated as the difference between the $\mathbf{4^{Me}}$ and $\mathbf{3^{Me}}$ in the presence of one or zero NH_3 molecules.

2.5. Theoretical Study on the Selectivity for NH_3

To rationalize the small molecule basic sensing properties of our Ni PW, it is critical to rationalize their ability to reversibly coordinate NH_3 and their selectivity when different molecules (NH_3 and H_2O) are also present in the solution. Therefore, it is interesting to focus on the nature of the coordinated molecule (NH_3 *vs* H_2O). We have previously reported that the addition of water to $\mathbf{2^H}$ leads to the formation of the paddlewheel complex $[Ni_2(\mathbf{Pn^H})_4(H_2O)]$ although coordination of H_2O seems to be far weaker.[22] Indeed, magnetic susceptibility measurements of the isolated materials always showed less than two unpaired electrons pointing toward a mixture of the aqua complex and $\mathbf{2^H}$. Moreover, as soon as ammonia is around, water is substituted to obtain $\mathbf{3^H}$. Quantum mechanical calculations were performed with $\mathbf{2^H}$ for the coordination of water. Similar to NH_3 as described above, the water molecule was considered to coordinate to $\mathbf{2^H}$ at the 4N- or 4S-side as well as in the paramagnetic or diamagnetic spin states. Results in Table 1 show that for H_2O coordination at the 4N-side, the HS state is again more stable than the LS by 2.08 kcal mol^{-1}. This small difference between the LS and HS state suggests that the interaction does not involve the rearrangement of the electrons in the Ni 3d molecule orbitals, but rather that a weak bonding takes place. Moreover, the preferred coordination site is the 4N-side which is more stable than the 4S-side by 8.74 kcal mol^{-1} for the HS state. This suggests that in the presence of both NH_3 and H_2O, competition for the same coordination site at $\mathbf{2^H}$ takes place. The small difference between the LS and HS state after water coordination at the 4N-side can explain the found magnetic data:[22] Some water molecules are coordinated to give the HS state and other water molecules give the LS state. The optimized structures for both spin states of $[Ni_2(\mathbf{Pn^H})_4(H_2O)]$ are displayed in **Figure 3**.

The most striking difference is observed in the Ni-O distances with 3.292 Å for the LS and 2.141 Å for the HS state. The shorter Ni-O distance observed in the low-spin (LS) complex compared to the high-spin (HS) complex contrasts with typical trends. This difference can be attributed to variations in the coordination environments: The LS complex adopts a square-pyramidal geometry,

Research Article
doi.org/10.1002/ceur.202500337

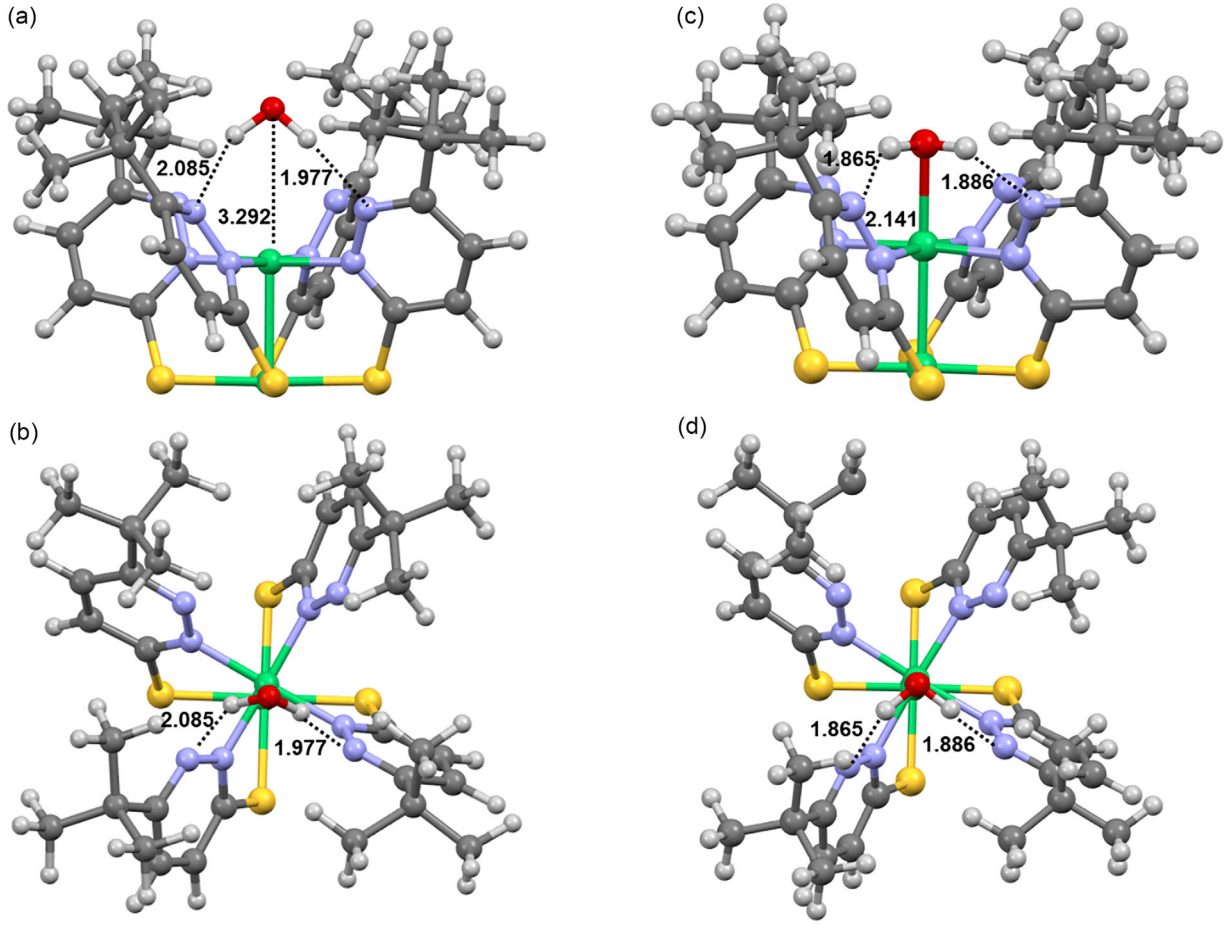

Figure 3. Optimized structures of the low spin state a,b) and high spin state c,d) of $[Ni_2(\mathbf{Pn^H})_4(H_2O)]$. Top row: views along the N4 plane; bottom row: views along the Ni–Ni axis. Yellow, lilac, gray, red, green and white spheres are S, N, C, O, Ni, and H atoms. Bond distances are in Å.

while the HS complex displays an octahedral configuration. The pentacoordination in the LS state and hexacoordination in the HS state are further supported by the Mayer Bond Order (MBO) index. In the LS state, the Ni–O bond order is below 0.1, indicating a negligible interaction, whereas the HS state shows an MBO of 0.4070 (Table S14, Supporting Information). Despite the different Ni-O distances and MBO indexes in the two systems, the binding energies are very similar (−13.84 and −11.76 kcal mol^{-1}, in the HS and LS states, respectively). This finding further supports our conclusion that the larger part of the binding energy value is due to the H-bond and not to the direct interaction of the small molecule with the Ni center, even for $[Ni_2(\mathbf{Pn^H})_4(H_2O)]$. The calculated binding energy in $[Ni_2(\mathbf{Pn^H})_4(H_2O)]$ for the more stable 4N-side in the HS state is −13.84 kcal mol^{-1}, which is 4.91 kcal mol^{-1} less stable than in $\mathbf{3^H}$, explaining the experimentally observed preference for NH_3 over H_2O. The stronger binding energy of the NH_3 with respect to water is certainly due to NH_3 being a better nucleophile which can be quantified with the condensed nucleophilic Fukui function f_k^-, (1.012 vs. 0.789 for N atom of NH_3 and O atom of water, respectively). Finally, similar trends are observed with the methylated system where the water molecule coordinates in $[Ni_2(\mathbf{Pn^{Me}})_4(H_2O)]$ (Table 1 and Figure S20, Supporting Information): preferred coordination at the 4N-side and lower binding energies for H_2O in comparison to NH_3 which is in agreement with the experiment where $[Ni_2(\mathbf{Pn^{Me}})_4(H_2O)]$ has not isolated. Similar observations regarding Ni–O bond distances and MBO indices for $[Ni_2(\mathbf{Pn^H})_4(H_2O)]$ also apply to complexes with Me substituents in both LS and HS states (Table S14, Supporting Information).

2.6. Fabrication into Thin Foils

The potential of $\mathbf{3^{Me}}$ as a NH_3 probe was investigated by fabricating it into a thin foil ($\mathbf{f\text{-}3^{Me}}$), similar to previously described $[Ni_2(\mathbf{Pn^H})_4]$ ($\mathbf{2^H}$).[40] However, due to the low solubility of $\mathbf{2^{Me'}}$, the ammonia–PW complex $\mathbf{3^{Me}}$ was encapsulated into the hydrogel Hydromed D4 and knife-coated to 7.5 µm thickness onto a gas-permeable poly(ethylene terephthalate) support. The foils are thin enough to be measured in transmission mode by a standard UV-Vis photometer. The typical red color of $\mathbf{3^{Me}}$ ($\lambda_{max} = 529$ nm dissolved in CH_2Cl_2) was observed as a broad absorption of weak intensity in $\mathbf{f\text{-}3^{Me}}$ at $\lambda_{max} = 520$ nm (**Figure 4**, red line).

In contrast to $[Ni_2(\mathbf{Pn^H})_4(NH_3)]$, soaking the foil of $\mathbf{f\text{-}3^{Me}}$ in H_2O worked quite poorly. After 3 h, the typical red color of the foil and its UV-Vis spectrum is essentially unchanged (Figure 4, blue line).

Research Article
doi.org/10.1002/ceur.202500337

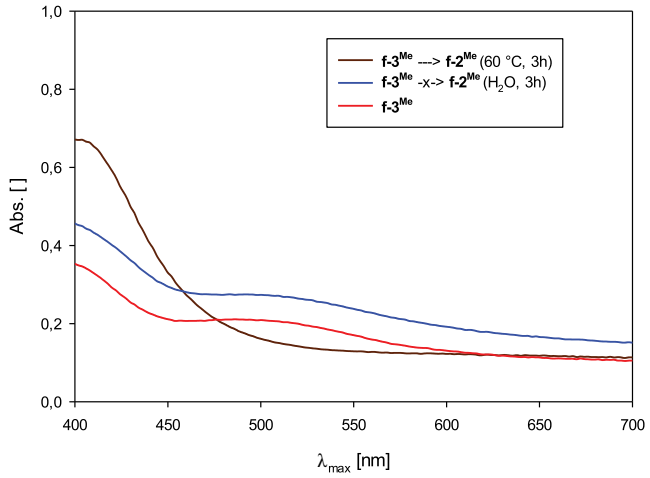

Figure 4. UV-vis spectra of encapsulated $\mathbf{3^{Me}}$ in hydrogel D4 (**f-3^{Me}**): red line: **f-3^{Me}** after fabrication; blue line: **f-3^{Me}** after soaking in H_2O; brown line: **f-3^{Me}** after heating to 60 °C.

Alternatively, heating the foil of **f-3^{Me}** to 60 °C for 3 h in an oven led to a color change to light-brown. In the UV-Vis spectrum, this resulted in the disappearance of the red color and the broad absorption at 520 nm (Figure 4, brown line). It remains unclear if the hexanuclear cluster of $\mathbf{2^{Me'}}$ is formed when encapsulated in the hydrogel foil (**f-2^{Me}**). Longer heating times (e.g., 1 day) or higher temperatures (e.g. 120 °C) led to the loss of the NH_3 sensing capabilities and the appearance of a yellowish color of the foil pointing towards decomposition. Overall, the removal of NH_3 from encapsulated **f-3^{Me}** requires more drastic conditions (60 °C, 3 h) than from encapsulated $[Ni_2(\mathbf{Pn^H})_4(NH)_3]$ (soaking in H_2O, 20 min).[40] Nevertheless, foils of **f-2^{Me}** revert to **f-3^{Me}** by simply soaking the foil in concentrated aqueous NH_3 solution, giving the same red color and spectral features. Therefore, also **f-3^{Me}** is in principle capable of reversibly losing and taking up NH_3. In contrast to the solution chemistry of $\mathbf{3^{Me}}$, encapsulated **f-3^{Me}** does not turn green upon exposure to gaseous NH_3 or prolonged soaking in aqueous NH_3, indicating that bis–ammine complex $\mathbf{4^{Me}}$ does not form in the foil.

3. Conclusion

The influence of ligand substituents in the $\mathbf{HPn^R}$ ligand family has drastic consequences on their coordination chemistry and the resulting vapochromic paddlewheel (PW) complexes. The previously published system where the ligand $\mathbf{Pn^H}$ exhibits a hydrogen atom in 4-position allowed isolation of both the PW complexes $[Ni_2(\mathbf{Pn^H})_4]$ and $[Ni_2(\mathbf{Pn^H})_4(NH_3)]$, including the study of their vapochromic behavior both in the molecular and encapsulated state. In contrast, the $\mathbf{Pn^{Me}}$ with a methyl group in 4-position leads initially to the formation of a macrocyclic, hexa–nuclear complex $[Ni_6(\mathbf{Pn^{Me}})_{12}]$ ($\mathbf{2^{Me'}}$) instead of the targeted PW complex $[Ni_2(\mathbf{Pn^{Me}})_4]$. Nevertheless, $\mathbf{2^{Me'}}$ showed vapochromism towards NH_3, resulting in a change of color and spin state, giving PW complex $[Ni_2(\mathbf{Pn^{Me}})_4(NH_3)]$ ($\mathbf{3^{Me}}$). Again in contrast to $[Ni_2(\mathbf{Pn^H})_4(NH_3)]$, $\mathbf{3^{Me}}$ showed further reactivity to NH_3, resulting in the highly unstable bis–ammine complex $[Ni(\mathbf{Pn^{Me}})_2(NH_3)_2]$ ($\mathbf{4^{Me}}$). Finally, for ligand $\mathbf{HPn^{tBu}}$, with a second *t*Bu group in 4-position, no PW complex is formed, but only the formal monomer of a PW complex, $[Ni(\mathbf{Pn^{tBu}})_2]$ ($\mathbf{6^{tBu}}$) is isolated. Our quantum mechanical calculations explain the preferential coordination to the Ni atom at the nitrogen (N) site over the sulfur (S) site. A key factor in this selectivity is the role of hydrogen bonding to the third donor site in the pyridazine ligand, which stabilizes coordination at the 4N-site and influences the overall geometry of the complex. Indeed, in absence of an additional nitrogen atom in the ligand, as modeled with pyridine substituents ($[Ni_2(\mathbf{Pn^{Py}})_4(NH_3)]$), no preference of the 4N- vs. the 4S-site is observed. Furthermore, the calculated binding energies of the complexes with NH_3 and H_2O confirm the high selectivity for ammonia of these systems due to stronger hydrogen bonds in the ammonia PW complex. This selectivity is particularly relevant for their potential application as sensors, where precise molecular recognition is essential. While still not yet applicable, this in-depth study contributes to a more comprehensive understanding of the behavior of these paddlewheel complexes, guiding experimental efforts and facilitating the development of novel sensor materials with enhanced performance.

Supporting Information

The authors have cited additional references within the Supporting Information.[64–75]

Acknowledgements

The authors gratefully acknowledge support from NAWI Graz.

Conflict of Interest

The authors declare no conflict of interest.

Author Contributions

Sebastian Rücker: investigation. **Jörg A. Schachner**: supervision; writing—original draft. **Sergey M. Borisov**: investigation. **Ferdinand Belaj**: investigation. **Silvia Carlotto**: investigation; formal analysis; writing—review & editing. **Lidia Armelao**: writing—review & editing. **Antoine Dupé**: investigation. **Nadia C. Mösch-Zanetti**: conceptualization; project administration; supervision; writing—review & editing.

Data Availability Statement

The data that support the findings of this study are available from the corresponding author upon reasonable request.

Research Article
doi.org/10.1002/ceur.202500337

Keywords: ammonia · nickel complexes · paddlewheel complexes · spin crossover · vapochromism

[1] *Multiple bonds between metal atoms* (Eds: F. A. Cotton, C. A. Murillo, R. A. Walton), Springer Science and Business Media **2005**.
[2] M. Köberl, M. Cokoja, W. A. Herrmann, F. E. Kühn, *J. Chem. Soc., Dalton Trans.* **2011**, *40*, 6834.
[3] N. J. Patmore in *Organometallic Chemistry* (Eds.: I. J. S. Fairlamb, J. M. Lynam), Royal Society of Chemistry **2010**, pp. 77–92.
[4] E. A. Hillard, *Curr. Inorg. Chem.* **2013**, *3*, 112.
[5] M. Cortijo, R. González-Prieto, S. Herrero, J. L. Priego, R. Jiménez-Aparicio, *Coord. Chem. Rev.* **2019**, *400*, 213040.
[6] J. Hansen, H. M. L. Davies, *Coord. Chem. Rev.* **2008**, *252*, 545.
[7] J. Campos, *Nat. Rev. Chem.* **2020**, *4*, 696.
[8] R. H. D. Lyngdoh, H. F. Schaefer, R. B. King, *Chem. Rev.* **2018**, *118*, 11626.
[9] M. Cortijo, P. Delgado-Martínez, R. González-Prieto, S. Herrero, R. Jiménez-Aparicio, J. Perles, J. L. Priego, M. R. Torres, *Inorg. Chim. Acta* **2015**, *424*, 176.
[10] C. Furlani, M. L. Luciani, *Inorg. Chem.* **1968**, *7*, 1586.
[11] M. Bonamico, G. Dessy, V. Fares, *Dalton Trans.* **1977**, *23*, 2315.
[12] M. Bonamico, G. Dessy, V. Fares, *J. Chem. Soc. D.* **1969**, *19*, 1107.
[13] C. Bellitto, G. Dessy, V. Fares, *Inorg. Chem.* **1985**, *24*, 2815.
[14] A. Kobayashi, T. Kojima, R. Ikeda, H. Kitagawa, *Inorg. Chem.* **2006**, *45*, 322.
[15] F. P. Dwyer, D. P. Mellor, *J. Am. Chem. Soc.* **1941**, *63*, 81.
[16] F. A. Cotton, M. Matusz, R. Poli, *Inorg. Chem.* **1987**, *26*, 1472.
[17] F. A. Cotton, M. Matusz, R. Poli, X. Feng, *J. Am. Chem. Soc.* **1988**, *110*, 1144.
[18] C. Lin, J. D. Protasiewicz, T. Ren, *Inorg. Chem.* **1996**, *35*, 7455.
[19] J. F. Berry, E. Bothe, F. A. Cotton, S. A. Ibragimov, C. A. Murillo, D. Villagran, X. Wang, *Inorg. Chem.* **2006**, *45*, 4396.
[20] J. B. Diccianni, C. Hu, T. Diao, *Angew. Chem., Int. Ed.* **2016**, *55*, 7534.
[21] G. A. Melson, N. P. Crawford, B. J. Geddes, *Inorg. Chem.* **1970**, *9*, 1123.
[22] G. A. Melson, P. T. R. P. Greene, *Inorg. Chem.* **1970**, *9*, 1116.
[23] S. A. Al-Jibori, A. R. Al-Jibori, H. A. Mohamad, A. S. Al-Janabi, C. Wagner, G. Hogarth, *Inorg. Chim. Actapp.* **2019**, *488*, 152.
[24] E. S. Raper, A. M. Britton, W. Clegg, *Inorg. Chim. Acta* **1989**, *166*, 171.
[25] K. Pang, J. S. Figueroa, I. A. Tonks, W. Sattler, G. Parkin, *Inorg. Chim. Acta* **2009**, *362*, 4609.
[26] T. R. Brown, B. S. Dolinar, E. A. Hillard, R. Clérac, J. F. Berry, *Inorg. Chem.* **2015**, *54*, 8571.
[27] M. P. Shores, C. M. Klug, S. R. Fiedler in *Spin-Crossover Materials: Properties and Applications* (Ed: M. A. Halcrow), John Wiley & Sons, Ltd. **2013**, pp. 281–301.
[28] M. M. Khusniyarov, *Chem. Eur. J.* **2016**, *22*, 15178.
[29] J. Larionova, L. Salmon, Y. Guari, A. Tokarev, K. Molvinger, G. Molnár, A. Bousseksou, *Angew. Chem., Int. Ed.* **2008**, *47*, 8236.
[30] S. Venkataramani, U. Jana, M. Dommaschk, F. D. Sonnichsen, F. Tuczek, R. Herges, *Science* **2011**, *331*, 445.
[31] M. Dommaschk, V. Thoms, C. Schütt, C. Näther, R. Puttreddy, K. Rissanen, R. Herges, *Inorg. Chem.* **2015**, *54*, 9390.
[32] S. Thies, H. Sell, C. Bornholdt, C. Schütt, F. Kohler, F. Tuczek, R. Herges, *Chem. Eur. J.* **2012**, *18*, 16358.
[33] S. Thies, H. Sell, C. Schütt, C. Bornholdt, C. Näther, F. Tuczek, R. Herges, *J. Am. Chem. Soc.* **2011**, *133*, 16243.
[34] P. Kar, M. Yoshida, Y. Shigeta, A. Usui, A. Kobayashi, T. Minamidate, N. Matsunaga, M. Kato, *Angew. Chem., Int. Ed.* **2017**, *56*, 2345.
[35] F. Röck, N. Barsan, U. Weimar, *Chem. Rev.* **2008**, *108*, 705.
[36] O. S. Wenger, *Chem. Rev.* **2013**, *113*, 3686.
[37] Y. J. Diaz, Z. A. Page, A. S. Knight, N. J. Treat, J. R. Hemmer, C. J. Hawker, J. R. de Alaniz, *Chem. Eur. J.* **2017**, *23*, 3562.
[38] M. E. Nikiforova, M. O. Talismanova, G. G. Aleksandrov, S. K. Kotovskaya, A. A. Sidorov, V. M. Novotortsev, V. N. Ikorskii, V. N. Charushin, I. L. Eremenko, I. I. Moiseev, *Russ. Chem. Bull.* **2006**, *55*, 2181.
[39] S.-D. Han, X.-H. Miao, S.-J. Liu, X.-H. Bu, *Dalton Trans.* **2015**, *44*, 560.
[40] K. M. Fürpaß, L. M. Peschel, J. A. Schachner, S. M. Borisov, H. Krenn, F. Belaj, N. C. Mösch-Zanetti, *Angew. Chem., Int. Ed.* **2021**, *60*, 13401.
[41] S. Holler, M. Tüchler, F. Belaj, L. F. Veiros, K. Kirchner, N. C. Mösch-Zanetti, *Inorg. Chem.* **2016**, *55*, 4980.
[42] M. Tüchler, F. Belaj, G. Raber, D. Neshchadin, N. C. Mösch-Zanetti, *Inorg. Chem.* **2015**, *54*, 8168.
[43] M. Tüchler, S. Holler, S. Rendl, N. Stock, F. Belaj, N. C. Mösch-Zanetti, *Eur. J. Inorg. Chem.* **2016**, 2609.
[44] S. Holler, M. Tüchler, B. G. Steller, F. Belaj, L. F. Veiros, K. Kirchner, N. C. Mösch-Zanetti, *Inorg. Chem.* **2018**, *57*, 6921.
[45] M. Tüchler, M. Ramböck, S. Glanzer, K. Zangger, F. Belaj, N. C. Mösch-Zanetti, *Inorganics (Basel).* **2019**, *7*, 24.
[46] C. Vidovič, L. M. Peschel, M. Buchsteiner, F. Belaj, N. C. Mösch-Zanetti, *Chem. Eur. J.* **2019**, *25*, 14267.
[47] B. Timmer, W. Olthuis, A. van den Berg, *Sens. Actuators, B.* **2005**, *107*, 666.
[48] F. Belaj, S. Rücker, J. A. Schachner, N. C. Mösch-Zanetti, *CSD Commun.* **2021**.
[49] Deposition numbers 2183407 (for $\mathbf{1^{Me}}$), 2183409 (for $\mathbf{2^{Mer}}$), 2183410 (for $\mathbf{3^{Me}}$), 2183411 (for $\mathbf{4^{Me}}$), 2183412 (for $\mathbf{5^{tBu}}$) and 2183414 (for $\mathbf{6^{tBu}}$) Contain the Supplementary Crystallographic Data for This Paper. These Data Are provided Free of Charge by the Joint Cambridge Crystallographic Data Centre and Fachinformationszentrum Karlsruhe Access Structures Service.
[50] B. Terfassa, C. Holzer, J. A. Schachner, P. Cias, H. Krenn, F. Belaj, N. C. Mösch-Zanetti, *J. Coord. Chem.* **2016**, *69*, 433.
[51] A. Nimthong-Roldán, J. L. Guillet, J. McNeely, T. J. Ozumerzifon, M. P. Shores, J. A. Golen, A. L. Rheingold, L. H. Doerrer, *Dalton Trans.* **2017**, *46*, 5546.
[52] S. A. Nikolaevskii, M. A. Kiskin, A. A. Starikova, N. N. Efimov, A. A. Sidorov, V. M. Novotortsev, I. L. Eremenko, *Russ. Chem. Bull.* **2016**, *65*, 2812.
[53] L. Zhu, X. Chen, Q. Zhao, Z. Li, X. Zhang, B. Sun, *Z. Anorg. Allg. Chem.* **2010**, *636*, 1441.
[54] F. A. Cotton, D. M. L. Goodgame, *J. Am. Chem. Soc.* **1960**, *82*, 5771.
[55] S. Trofimenko, J. C. Calabrese, J. K. Kochi, S. Wolowiec, F. B. Hulsbergen, J. Reedijk, *Inorg. Chem.* **1992**, *31*, 3943.
[56] I. V. Ershova, I. V. Smolyaninov, A. S. Bogomyakov, M. V. Fedin, A. G. Starikov, A. V. Cherkasov, G. K. Fukin, A. V. Piskunov, *Dalton Trans.* **2019**, *48*, 10723.
[57] B. J. McNicholas, Z. J. Tong, D. Bím, R. F. Turro, N. P. Kazmierczak, J. Chalupský, S. E. Reisman, R. G. Hadt, *Inorg. Chem.* **2023**, *62*, 14010.
[58] D. Ghorai, A. Garcia-Roca, B. L. Tóth, J. Benet-Buchholz, A. W. Kleij, *Angew. Chem., Int. Ed.* **2023**, *62*, e202314865.
[59] R. G. Parr, W. Yang, *J. Am. Chem. Soc.* **1984**, *106*, 4049.
[60] I. Kour, G. Kour, R. Sachar, S. Anthal, R. Kant, *J. Mol. Struc.* **2017**, *1128*, 769.
[61] A. Malloum, J. Conradie, *J. Mol. Liquids* **2021**, *336*, 116199.
[62] M. Bogojeski, L. Vogt-Maranto, M. E. Tuckerman, K.-R. Müller, K. Burke, *Nat. Commun.* **2020**, *11*, 5223.
[63] A. J. Bridgeman, G. Cavigliasso, L. R. Ireland, J. Rothery, *J. Chem. Soc., Dalton Trans.* **2001**, *14*, 2095.
[64] G. M. Sheldrick, *Acta Cryst.* **2008**, *A64*, 112.
[65] G. M. Sheldrick, *Acta Cryst.* **2015**, *C71*, 3.
[66] J. P. Perdew, *Phys. Rev. B.* **1986**, *33*, 8822.
[67] A. D. Becke, *Phys. Rev. A.* **1988**, *38*, 3098.
[68] S. Grimme, S. Ehrlich, L. Goerigk, *J. Comput. Chem.* **2011**, *32*, 1456.
[69] F. M. Bickelhaupt, E. J. Baerends, in *Reviews in Computational Chemistry* (Eds: K. B. Lipkowitz, B. D. Boyd), Wiley-VCH Weinheim **2000**, pp. 1–86.
[70] M. Mitoraj, A. Michalak, *Organometallics* **2007**, *26*, 6576.
[71] F. Neese, *WIREs Comput Mol Sci.* **2022**, *12*, e1606.
[72] F. Weigend, *J. Comput. Chem.* **2008**, *29*, 167.
[73] S. Grimme, J. Antony, S. Ehrlich, H. Krieg, *J. Chem. Phys.* **2010**, *132*, 154104.
[74] J. P. Perdew, R. G. Parr, M. Levy, *Phys. Rev. Lett.* **1982**, *49*, 1691.
[75] W. Yang, W. J. Mortier, *J. Am. Chem. Soc.* **1986**, *108*, 5708.

Manuscript received: August 27, 2025
Version of record online: